

ČESKÉ VYSOKÉ UČENÍ TECHNICKÉ V PRAZE  
FAKULTA DOPRAVNÍ

CZECH TECHNICAL UNIVERSITY IN PRAGUE  
FACULTY OF TRANSPORTATION SCIENCES

doc. Ing. Ondřej Jiroušek, Ph.D.

MODERNÍ METODY VE VÝZKUMU TRABEKULÁRNÍ KOSTI A JEJICH  
VYUŽITÍ VE TKÁŇOVÉM INŽENÝRSTVÍ

MODERN METHODS IN TRABECULAR BONE RESEARCH AND THEIR  
UTILIZATION IN TISSUE ENGINEERING

## Summary

Trabecular bone, also known as cancellous or spongy bone, is one of the two osseous tissues (compact and spongional) that form the human skeletal system. The skeletal system is very important not only as a supportive structure for muscles and other soft tissues, but also plays non-substitutable role as a protection of inner organs. Other functions performed by the osseous tissue are: calcium phosphate storage and hemopoiesis, i.e. formation of blood cellular components in bone marrow. From the material science point of view trabecular bone is a highly organized composite material, with very unique properties. Although the effort to replace autograft and allograft bones by a synthetic tissue-engineered scaffold has continued for the last two decades there are still several open issues that need to be addressed.

In this work an engineering approach is used to assess the microstructural and mechanical properties of trabecular bone and to show the possibilities of modern experimental, numerical and imaging methods for quantification of bone quality. There are several areas in which the results of the research can be utilized: i) early diagnosis of osteoporosis and bone quality and quantity measurements, ii) bone fracture risk assessment, iii) evaluation of performance of artificial implants, iv) design of bone scaffold, v) efficacy comparison of different drug therapies and treatments for osteoporosis, vi) in vivo assessment of changes in bone due to osteoporosis using in-vivo animal testing.

Combination of experimental and numerical methods is used to measure the quality of trabecular bone given in terms of material performance, i.e. standard mechanical properties (stiffness, strength, yield stress and yield strain, hardening modulus) are evaluated inversely using microstructural finite element models with tissue material properties measured by nanoindentation. To compare the results of numerical simulations to the response of real trabecular bone under mechanical load a unique experimental setup has been developed which enables to capture the deforming microstructure in great detail. A custom loading device enabling to gradually compress a sample directly inside micro-CT chamber has been designed. This enables to capture individual deformation states of the sample and thus direct comparison between experimental and numerical results.

These methods enable not only to assess the relationship between the microstructural parameters and the overall bone mechanical properties but also give us the opportunity to compare *nondestructively* mechanical properties of newly formed bone in animal models (provided that some information about the tissue properties is known) and in case of successful immobilization of the animal even *in-vivo*. As an example of such possibilities, an attempt to inversely estimate the bone quality using microstructural models has been made in which voxel models based on images from microfocus computed tomography were used to compare the overall stiffness of rat vertebrae. Possibility to use the micromechanical models developed from micro-CT data to estimate the performance of a proposed orthopaedic therapy is outlined. The advantage of such an approach is demonstrated using an example of stem cell therapy, when a bone scaffold combined with human mesenchymal stem cells is used in a rat model of vertebral body defects.

## Souhrn

Trabekulární kost, která se také nazývá spongiózní (houbovitou) kostí, je jedním druhem kostní tkáně. Soubor všech kostí vytváří kostru, neboli skelet. Skeleton je velmi důležitý nejen jako podpůrná konstrukce pro svaly a další měkké tkáně, ale hraje taky nezastupitelnou roli jako ochrana pro vnitřní orgány. Mezi další funkce můžeme zahrnout funkci zásobárny vápníku a hematopoézu, tedy tvorbu krevních buněčných komponent, která u dospělého člověka probíhá ve stromatu červené kostní dřeně. Z pohledu materiálového inženýrství je trabekulární kost vysoce hierarchický kompozitní materiál s velmi unikátními vlastnostmi. Ačkoliv úsilí zaměnit autograftový i alograftový materiál synteticky vyrobeným podpůrným skeletem bylo předmětem systematického bádání posledních dvou dekad, množství otázek stále zůstává otevřeno.

V této práci je použito inženýrského přístupu pro stanovení mikrostrukturálních a mechanických vlastností trabekulární kosti a k demonstraci možností moderních experimentálních, numerických a zobrazovacích metod pro stanovení kvality kosti. Výsledky tohoto výzkumu mohou najít uplatnění v následujících oblastech: i) včasná diagnostika osteoporózy a stanovení kvality a kvantity kostní hmoty, ii) kvantifikace rizika vzniku osteoporotické zlomeniny, iii) stanovení chování umělých náhrad, iv) návrh podpůrného skeletu, v) porovnání efektivnosti různých postupů a léků pro prevenci a léčbu osteoporózy, vi) stanovení postupných změn ve struktuře kosti v důsledku osteoporózy *in vivo* pomocí laboratorních zvířat.

Pro stanovení kvality trabekulární kosti je v práci použito kombinace experimentálních a numerických metod, kdy kvalita je vyjádřena pomocí standardních mechanických vlastností (tuhost, pevnost, mez kluzu, modul zpevnění). Tyto mechanické vlastnosti jsou určeny inverzně pomocí mikrostrukturálních MKP modelů s konstitutivními vztahy na úrovni jednotlivých trabekul, které jsou stanoveny pomocí nanoindentace. Výsledky těchto simulací jsou porovnány s odezvou vzorku trabekulární kosti, který je podroben jednoosé tlakové zkoušce v unikátním experimentálním zařízení, které umožňuje detailně zobrazit deformující se mikrostrukturu vzorku. Pro tyto účely bylo vyvinuto zatěžovací zařízení, které umožňuje postupné přitěžování vzorku v mikro-CT za současného ozařování a tak zachytit jednotlivé deformační stavy vnitřní struktury vzorku a tím i přímé porovnání experimentálních výsledků s numerickou simulací.

Tyto metody umožňují nejen odhalit vztah mezi mikrostrukturou a celkovými mechanickými vlastnostmi kosti, ale umožňují *nedestruktivně* porovnat mechanické vlastnosti nově tvořené kosti v experimentálních modelech laboratorních zvířat. Jako příklad možnosti vyžití náročných MKP simulací pro stanovení kvality kosti pomocí inverzního výpočtu je v práci demonstrován výpočet tuhosti páteřního obratle laboratorní krysy. Smysl těchto výpočtů tkví v možnosti porovnání úspěšnosti léčebného postupu, testovaného na laboratorním zvířeti a to, v případě úspěšného znehybnění, dokonce *in-vivo*. Využití detailních mikrostrukturálních modelů vytvořených ze snímků mikrofokální počítačové tomografie za účelem zhodnocení navržené ortopedické terapie je nastíněn v závěru práce. Uvedený příklad byl součástí většího výzkumu z oblasti využití kmenových buněk, kdy kostní podpůrný skelet kombinovaný s mesenchymálními kmenovými buňkami byl použit v modelu defektů páteřního obratle.

**keywords**

trabecular bone, micromechanical testing, nanoindentation, micro-CT, finite element method, bone scaffold, inverse modelling, tissue engineering

**klíčová slova**

trabekulární kost, mikromechanické zkoušení materiálů, nanoindentace, mikro-CT, metoda konečných prvků, kostní podpurný skelet, inverzní modelování, tkáňové inženýrství

# Contents

<b>1</b>	<b>Introduction</b>	<b>6</b>
1.1	Bone composition . . . . .	6
<b>2</b>	<b>Nanoindentation</b>	<b>7</b>
2.1	FE modelling of the nanoindentation experiment . . . . .	9
<b>3</b>	<b>Micromechanical testing</b>	<b>11</b>
3.1	Introduction . . . . .	11
3.2	Microscale three point bending . . . . .	11
3.3	Displacement tracking a strain calculation . . . . .	12
3.4	Microscale three-point bending . . . . .	13
3.5	Inverse calculation of material properties - fitting the response curve using FE modelling . . . . .	15
<b>4</b>	<b>Microstructural models</b>	<b>16</b>
4.1	Morphometric indices used in trabecular bone research . . . . .	16
4.2	Time-lapse micro-CT . . . . .	17
<b>5</b>	<b>Digital volume correlation</b>	<b>19</b>
<b>6</b>	<b>Inverse estimation of whole bone stiffness</b>	<b>22</b>
6.1	Voxel and tetrahedral micro-FE models . . . . .	22
6.2	Micro-FE models of whole bones . . . . .	23
6.3	Development of the micro-FE voxel model of rat vertebra . . . . .	24
6.4	Inverse calculation of the vertebral body stiffness . . . . .	24
6.5	Parallel PCG solver . . . . .	25
6.6	Experimental evaluation of the vertebral stiffness . . . . .	25
<b>7</b>	<b>Conclusions</b>	<b>26</b>
	<b>Bibliography</b>	<b>28</b>

# 1 Introduction

Trabecular bone is one of the two type of mineralized osseous tissue, that form our skeleton. Generally, two types of bone tissue, trabecular and cortical are present in any type of bone. Cortical bone is the dense layer on the surface of bones, while trabecular bone is the highly porous structure inside the ends of all long bones (e.g. femur, humerus or tibia). It is also present in other bones (e.g. in vertebral bodies) where it contributes to the overall strength of whole bones, namely under impact loads. At molecular level cortical and trabecular bone are made of the same constituents but their macroscopical, namely mechanical properties are quite different.

Since bone is a composite material, its properties are influenced by the properties of its constituents. Material properties of trabecular bone are furthermore heavily influenced by the architecture and connectivity of individual trabeculae. At molecular level one can consider bone to be a composite material consisting of organic and inorganic constituents. To establish the relationship between the overall mechanical properties and the microstructure, it is necessary to measure reliably the properties of individual trabeculae. This is quite challenging because of the small dimensions of trabeculae and their irregular shape. The length of trabecula is around 1 mm but it varies in different anatomical locations and species. The very small dimensions of trabeculae introduce special requirements on both experimental and numerical methods for mechanical properties assessment.

## 1.1 Bone composition

Bone is a natural composite material made of collagen matrix stiffened by crystalline salts composed primarily of calcium and phosphate. Collagen is a soft organic material and a fibrous protein also found in other connective tissues. The collagen provides the bone with toughness (while the inorganic salts are responsible for the rigidity and stiffness of the bone). Apart from collagen, there are other proteins present in the bone. These include glycoproteins and proteoglycans which create an amorphous mixture of extracellular material. In addition to this protein constituent of bone, there is inorganic constituent, which is a mineral very similar to hydroxyapatite – a naturally occurring mineral form of calcium apatite described chemically as  $\text{Ca}_{10}(\text{PO}_4)_6(\text{OH})_2$ .

The collagen molecules and crystals of hydroxyapatite are assembled into microfibrils. Further on, these fibrils create fibres with thickness about 3 to 5  $\mu\text{m}$ . The fibres are then assembled either randomly into woven bone or are organized into lamellae forming lamellar bone. These lamellae can be either in concentric groups, called osteons or can form linear lamellar groups, called plexiform bone. This level is called microstructural level.

At the same level, the bone is differs also in terms of its architectural organization. There are two types of architectural arrangement present in all types of bones. A thin layer of dense bone

covers all types of bones and is called cortical or compact bone. Under this dense layer in all weight-bearing bones there is a less dense type of bone, called trabecular or spongy bone. This bone is subject of this work. Application of modern imaging, experimental and numerical techniques for investigation of trabecular bone material properties is discussed in the forthcoming text.

## 2 Nanoindentation

Although there is a number of experimental techniques for measurement of bone tissue mechanical properties there are possibly five main methods used for this purpose: (i) tensile or three- (four-) point bending tests, (ii) buckling studies, (iii) acoustic methods, (iv) back-calculation from finite element simulations, (v) nanoindentation. The published results differ significantly, for any of the before-mentioned methods, even when the same testing protocol has been used by different research groups. There are several reasons for the scatter in the obtained results which can be attributed to different protocols used in sample preparation, different testing methods or the scatter can be explained by the real anisotropy and asymmetry of mechanical properties of the tissue itself. One of the most favourite methods used to measure the bone material properties is nanoindentation.

Nanoindentation has been used to measure the mechanical properties of both cortical and trabecular bone. For the cortical bone, this technique has been used to measure the properties from the level of single osteons. This technique has been used to identify the sources of material anisotropy of cortical bone and to explain the structure-property relationships in bone. It has been shown, that material properties measured by nanoindentation, vary even within completed secondary osteons [1]. Also, the elastic material properties (Young's modulus and hardness) are highest in the centre of the osteon and are declining outwards. Moreover, the mechanical properties of osteons were also found lower than those of the interstitial bone. Similar results were acknowledged by other authors, although some of them reported no statistically significant difference in material properties of osteons and interstitial bone [2]. Apart from this variation, nanoindentation has been used to show the anisotropy of human osteons [3]. In their work, nanoindentation was used to measure the principal material orientations with respect to its axis and to show that osteons are generally stiffer in longitudinal direction and that the principal direction of stiffness is slightly rotated from the osteon axis.

For the trabecular bone, nanoindentation has been extensively used in the last two decades. Similarly to cortical bone, variations in mechanical properties between samples harvested from different anatomical sites has been shown to be statistically significant [4, 5]. Among other documented factors, influencing the material properties, water and mineral content [6] have significant effect on properties of bone tissue, and this applies also to elastic modulus and hardness of human trabecular bone lamellae [7]. The water content has been shown to influence not only the elastic, but namely the viscous, yield and post-yield properties [8] of both cortical and

trabecular bone.

Although the nanoindentation is well established method for measuring elastic properties of trabecular bone, it is not so straightforward to use this method to measure its yield and post-yield properties. It is even more tricky to interpret the indentation results for materials that exhibit significant viscous (or poroelastic) deformation behaviour. One has to bear in mind that all biological materials exhibit viscous deformation behaviour. Therefore, while it is relatively easy to apply nanoindentation to obtain elastic properties of dry bone samples, both cortical and trabecular, to obtain viscoelastic (or elastic-viscoplastic) properties of bone introduces great difficulties not only for sample preparation and keeping the sample in physiological saline solution during the testing, but also for proper results interpretation.

Nanoindentation was developed in the mid 1970s and measures the hardness of a material in a small volume of interest. The principle of the method is same as in the traditional (macro)indentation test - a sharp tip of hard material is pressed down into a surface of the tested material and from the measured load and indentation area the hardness is calculated. Elastic properties of the material are evaluated using the Oliver-Pharr method, which uses the slope of the unloading part of the nanoindentation curve. This method assumes the material to be elastic and incompressible, the contact between the specimen and indenter purely Herizian and the unloading fully elastic. The method has been proven valid for axisymmetric indenters with infinitely smooth profile and perfect geometry, zero adhesive forces, frictionless contact and specimen represented by infinite half-space [9, 10].

The Young's modulus of the tested material is calculated from the unloading part of the indentation: the slope of the curve,  $dF/dh$  ( $F$  is the measured force and  $h$  is the indentation depth), upon unloading is indicative of the contact stiffness  $S$  which can be used to calculate the so-called reduced Young's modulus  $E_r$ :

$$E_r = \frac{1}{\beta} \frac{\sqrt{\pi}}{2} \frac{S}{\sqrt{A_p(h_c)}}, \quad (2.1)$$

in which the projected area of the indentation  $A_p(h_c)$  is fitted by a polynomial for a given contact depth  $h_c$ , and  $\beta$  is a geometrical constant. The reduced modulus  $E_r$  is then used to calculate the Young's modulus of the tested material  $E_m$  from the known Young's modulus of the indenter  $E_i$  using a simple relationship from contact mechanics:

$$\frac{1}{E_r} = \frac{(1 - \nu_i^2)}{E_i} + \frac{(1 - \nu_s^2)}{E_m}. \quad (2.2)$$

Usually, diamond is used for the indenter tip and (known) material properties of the indenter are then  $E_i = 1140$  GPa and  $\nu_i = 0.07$ . For common metal materials, the indentation hardness correlates linearly with both the yield strength and tensile strength [11]. For other materials including bone there is no correlation between the yield properties and hardness. However, constants for nonlinear material model can be obtained by fitting procedure for which a FE model of the indentation is developed and the constants of the chosen constitutive model are



obtained using an iterative approach. For each set of the material constants, the load-penetration curve is inversely calculated in the FE simulation and compared to the experimentally obtained one. The constants are varied and least squares approach is used to find the best fit between the experimentally and numerically obtained  $F - u$  curves.

## 2.1 FE modelling of the nanoindentation experiment

To obtain the constants of elasto-plastic material model with isotropic hardening from a large set of indentation curves from quasi-static nanoindentation following experiment has been carried out. Small cubic sample of trabecular bone was harvested from cadaveric human proximal femur (72 year old male). For the indentation, two peak forces, 10 mN and 20 mN were used in a grid of 20 indents. Each grid represented a set of different parameters: three different loading rates (20, 120, 240 mN/min) and three holding times (10, 20, 40 s) were used, each for the two peak forces.

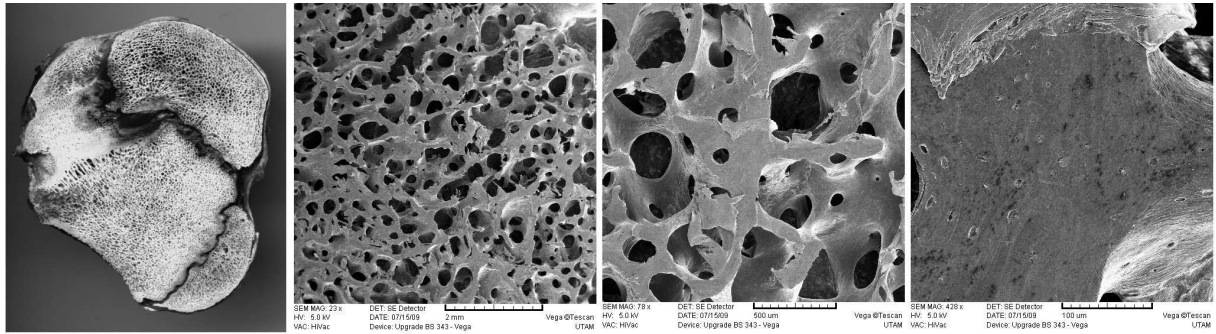


Figure 2.1: The microstructural arrangement of trabecular bone in the greater trochanter region (proximal femur).

In the inverse FE analysis a rotationally axisymmetric model of the indenter and the underlying bone was modelled. The Bercovich indenter with actual pyramidal shape was transformed into an equivalent cone. In spite of the nonlinear contact between the sample and the indenter, the sharp tip of the cone was rounded with radius  $r=200$  nm [12]. Both triangular and rectangular elements with quadratic shape functions were used to discretize the geometry (see Fig. 2.2). The contact between the indenter and the bone surface was assumed as frictionless.

The optimization algorithm used for inverse determination of material model can be described as follows: First, random values of material constants in expertly established within initial ranges and used for the initial simulation. The least squares method is used to calculate the  $R^2$  errors between numerical and experimental results and compared with a user specified threshold value. If the threshold is reached the ranges of material constants are modified for the next iterations. Each iteration in the optimization scheme consists of approximately 100 simulations and finally new  $R^2$  errors are calculated and sorted in decreasing order. Three highest values are used in the next iteration step and new sets of constants are generated using Gaussian distribution function. The best fit of the material constants is determined when limited number of iterations is reached.

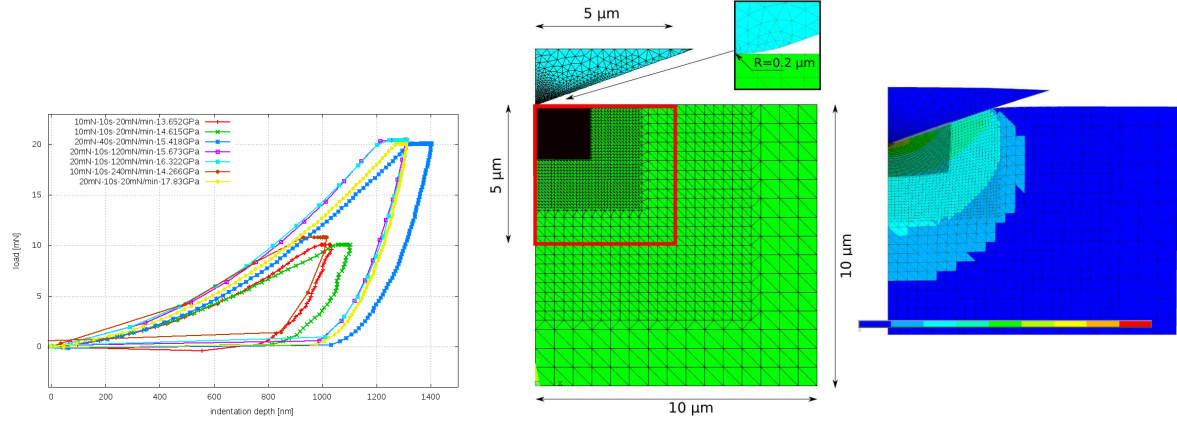


Figure 2.2: Example of the set of nanoindentation curves and FE model of the problem used for the inverse estimation of material properties.

To fit the experimentally obtained indentation curves a finite number of points is generated and the curves are sampled at the points.  $F-u$  pairs computed inversely and assessed experimentally are compared at these points using least squares approach. Resulting set of four material parameters ( $\mu$ ,  $E$ ,  $\sigma_Y$ ,  $E_{tan}$ ) is obtained as the best fit. The flowchart of the optimization scheme used in the back-calculation is given in Fig. 2.3. For the detailed description of the fitting algorithm and for the results obtained see [13, 14].

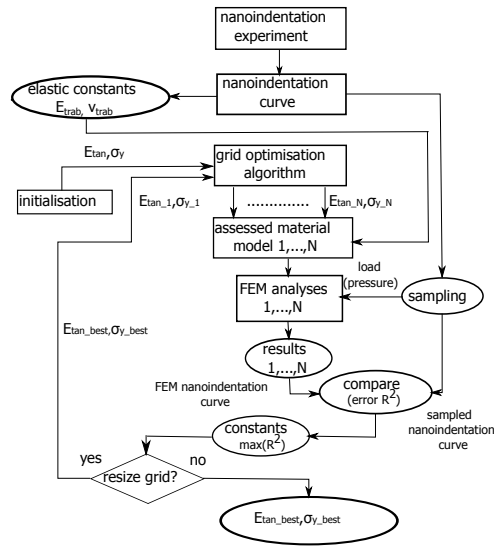


Figure 2.3: Flowchart of the optimization - fitting the parameters of the elasto-plastic material model by comparison of indentation curves.

## 3 Micromechanical testing

### 3.1 Introduction

To measure the material properties of individual trabeculae, there is one, probably more straightforward method to measure the mechanical properties *directly*. Despite the very small dimensions of the trabeculae it is possible to apply standard testing methods, i.e. three- or four-point bending, tension and compression tests to establish the stress-strain relationship for extracted trabecula. However, the delicate dimensions of the trabeculae and the microstructural arrangement of the trabeculae into a complicated network require that special care and special techniques must be used not only during the sample preparation and handling, but great care must be paid to evaluate the strains and stresses in the loaded sample. The main advantage of direct micromechanical testing compared to nanoindentation is the possibility to measure the yield properties directly or to measure at variable strain rates.

For a material model that would properly describe the elastic-plastic deformation as well as microdamage initiation and accumulation it is very important to introduce a damage model to microstructural FE (micro-FE) models. These models, built from very accurate three-dimensional image data acquired by micro-CT scanning are used to predict the overall properties of bone using samples with dimensions of several mm. It has been shown, that these models are able to predict the overall orthotropic *elastic* properties [15], both in dry and wet conditions [16] but fail to predict the yield properties and the softening behavior of trabecular bone. To describe properly behaviour of trabecular bone beyond the yield point, linear elastic description is (of course) insufficient and more advanced material model is needed.

### 3.2 Microscale three point bending

Nanoindentation has been successfully used to measure the elastic properties of trabecular bone both in dry and wet conditions [17, 18, 19]. It can be considered as the de-facto standard technique when only elastic properties are sought. When deformation behaviour beyond the yield point is important, it is more appropriate to use “standard” methods, e.g. three-point bending or tension. The only complication with these methods originates from the tiny dimensions of the samples. Usual length of a trabecula from great trochanter region is about 1 mm and the diameter is about 100  $\mu\text{m}$ . The dimensions of the samples require not only special harvesting and handling protocol, but also additional requirements are on the side of force measurement accuracy and consideration of the specimen geometry.

One of the options how to assess the exact 3D geometry of the specimen is to perform complete micro-CT scanning for each specimen prior the testing. This would require an extra time in which the specimen is irradiated by the X-rays during which the specimen undergoes drying and deproteinization since complete tomography is needed. Instead of using X-rays it is possible

to use visible light and construct the geometry using shape from silhouettes approach. This algorithm uses the so-called *visual hull*, i.e. intersection of the silhouettes taken from different view angles.

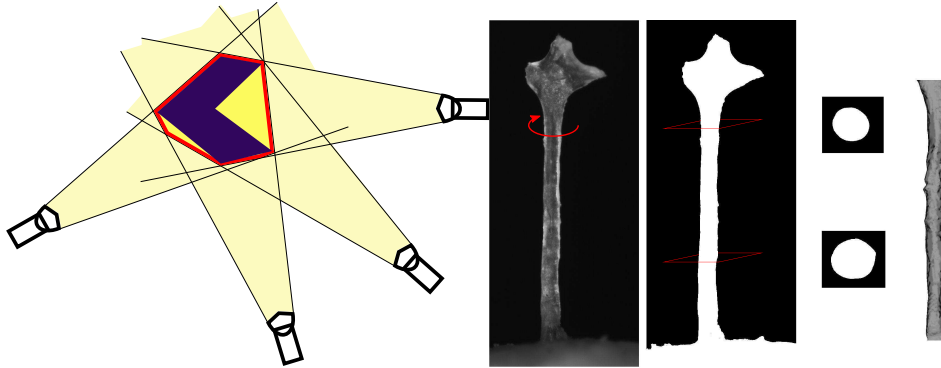


Figure 3.1: Principle of the shape-from-silhouettes method: a) visual hull - the intersection of the cones defines the bounding geometry of the object, b) trabecular sample and the reconstruction of its geometry from the shades.

For any silhouette image of an object (shade), we know that the object lies inside the volume generated by back-projecting the silhouette area. For the back-projection, only the geometrical parameters (distance from the camera to the object) are needed. If the object to be reconstructed is convex, this algorithm can reconstruct its shape with sufficient accuracy, provided that the background can be correctly subtracted from the images. This approach is used in our experiments. The object (extracted trabecula) is placed on a rotating table and diffuse light is used to illuminate it. In each angle, the shade is captured with high-resolution CCD camera and using a binary threshold separated from the background. Prior the testing, the accuracy of the method has been tested using a set of 5 samples and compared to the results obtained by X-ray microtomography. The difference between the reconstructed volumes was not larger than 4%.

### 3.3 Displacement tracking a strain calculation

Due to the delicate dimensions of the samples it is not possible to use contact method, e.g. strain gauge, for strain measurements. On the other hand, it is possible to use a contact-less optical methods to track the displacements on the surface of the sample and from the displacements calculate the strains. To measure the strains in the loaded sample one can use either high-resolution CCD camera and observe the deforming sample in visible light or take advantage of using X-rays and capture the projections using high-resolution X-ray detector. Using X-rays overcomes one problem with visible light - the object is very small and a microscope must be used to get sufficient magnification. With increasing magnification, the depth of focus is decreasing. Due to the curved surface of the samples marginal regions of the sample are out of focus which can cause problems in correlation at that area.

To track the displacements a method based on maximalization of the correlation coefficient between two sub-images is used. A set of points (defining the grid) is defined in the undeformed

(reference) image. Around each of the points a rectangular neighbourhood is defined forming a subimage  $I_0$ . The reference image subset is then shifted and deformed and compared to the image subset in the deformed image  $I_1$ . The best correlation between  $I_0$  and  $I_1$  is sought by nonlinear optimization algorithm (inverse compositional algorithm). The cross correlation coefficient used in the minimization algorithm  $r_{ij}$  is defined as:

$$r(u, v, \frac{\partial u}{\partial x}, \frac{\partial u}{\partial y}, \frac{\partial v}{\partial x}, \frac{\partial v}{\partial y}) = 1 - \frac{\sum_i \sum_j [I_0(x_i, y_j) - \bar{I}_0][I_1(x'_i, y'_j) - \bar{I}_1]}{\sqrt{\sum_i \sum_j [I_0(x_i, y_j) - \bar{I}_0]^2 \sum_i \sum_j [I_1(x'_i, y'_j) - \bar{I}_1]^2}}. \quad (3.1)$$

Here  $I_0(x_i, y_i)$  is the pixel intensity at a point  $(x_i, y_i)$  in the reference (undeformed) image and  $I_1(x_i, y_j)$  is the intensity at a point  $(x'_i, y'_j)$  in the deformed image. The mean intensity values in matrices  $I_0$  and  $I_1$  are represented by the overbarred symbols  $\bar{I}_0$  and  $\bar{I}_1$ .

When the linear transformation between the reference and deformed subset is found, it is easy to compute directly the strain tensor. It can be readily shown, that the coefficient of the linear affine transformation

$$\begin{aligned} x' &= x + u + \frac{\partial u}{\partial x} \Delta x + \frac{\partial u}{\partial y} \Delta y \\ y' &= y + v + \frac{\partial v}{\partial x} \Delta x + \frac{\partial v}{\partial y} \Delta y \end{aligned} \quad (3.2)$$

are members of the deformation gradient tensor  $F$ . In equation 3.2 translations of the centre of the subimage  $u$  and  $v$  as well as the distances  $\Delta x$  and  $\Delta y$  from the centre of the subimage to the point  $(x, y)$  are defined in the image coordinate system  $(x, y)$ . Thus, the correlation coefficient  $r_{ij}$  is only a function of displacement components and displacement gradients. Arranging the displacement gradients in the deformation tensor  $F = F_{ik} = \delta_{ik} + \frac{\partial u_i}{\partial x_k}$ , the Green-Lagrange strain tensor can be then computed as:

$$E = \frac{1}{2}(F^T F - I). \quad (3.3)$$

For fitting the response curves, the Green-Lagrange strain tensor does not need to be evaluated, only the displacements are used to fit the complete  $F - u$  response. But the G-L strain tensor is used to compare the numerical and experimental results.

### 3.4 Microscale three-point bending

To mechanically test trabeculae using a miniaturized version of three-point bending experimental setup (Fig. 3.2) was developed using precise translation stages (Standa Ltd., Lithuania) with  $1 \mu\text{m}$  sensitivity. For the loading a high precision linear stage (M-UMR3.5, Newport Corp., USA) with differential micrometer (DM11-5, Newport Corp., USA) with  $0.1 \mu\text{m}$  sensitivity and 5 mm travel range was used. Applied force is measured using 2.2 N load sensor (FBB350, FUTEK Advanced Sensor Technology Inc., USA). For optical measurement of deformations the setup is equipped

with a high-resolution CCD camera attached to an optical microscope (Navitar Inc., USA). This configuration enables to acquire images of the sample under slowly increasing load and to use tracking of markers defined in the reference image to measure the displacements and strains in the samples.

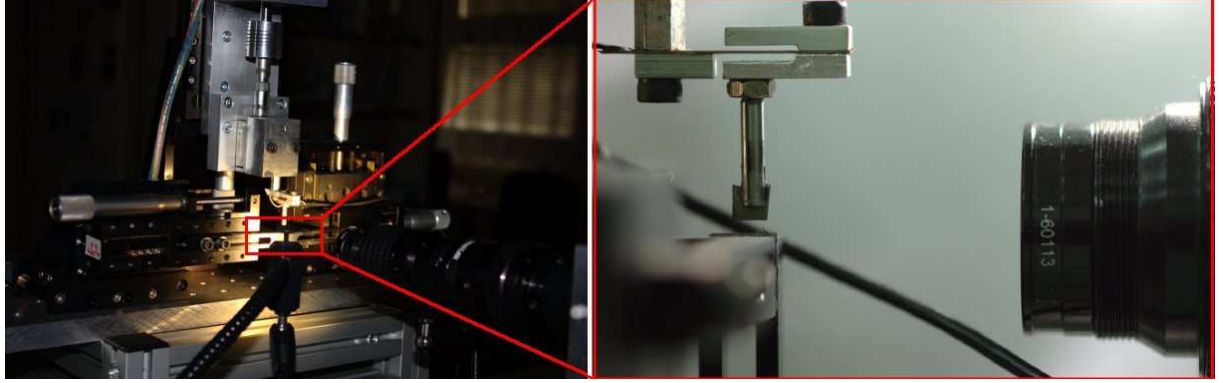


Figure 3.2: Experimental setup used in the three-point bending of extracted human trabeculae: a) general view of the experimental arrangement showing the micropositioning tables and loading device controlled by stepper motors, b) closer view showing the sharp loading tip and the miniature load cell.

The samples were extracted under magnifying glass ( $4 \times$  magnification) from the same proximal human femur (Fig. 4) as used in the nanoindentation experiment using a sharp-tip scalpel and pair of tweezers. Trabeculae were cleaned off marrow and grease in a detergent. Ultrasonic bath was used in short time intervals.

To overcome the problems with shallow focal depth one can use, instead of the visible light, X-rays. This has a motivation in the improvement of displacement tracking accuracy. As markers to be tracked gold coated borosilicate hollow microspheres were used. Gold was selected due to its high atomic number ( $Z_{Au} = 79$ ). The microspheres were covered with 250 nm golden layer and the diameter of the spheres was  $5 - 15 \mu\text{m}$  (Microsphere Technology Ltd., Ireland). The microspheres were used to create a random pattern on the surface of the specimens using a solution of phosphate buffered saline (pH 7.0). Added glycerine caused almost perfect adhesion to the samples' surface.

Similar experimental setup was used inside the X-ray shielded box. Each specimen was tested in three-point bending while X-ray microradiography was used to track the displacements in the loaded specimen. Positions of the microspheres were identified using a circular Hough transformation. The positions of the centres of markers were used in consequent strain calculations. An illustrative example of radiographs showing the three types of markers is depicted in Fig. 3.3. More on the experiment can be found in [20].

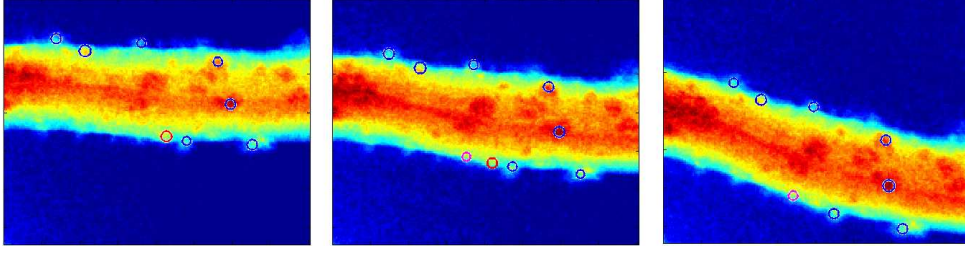


Figure 3.3: Radiographs of loaded trabecula (6, 50, 200  $\mu\text{m}$  midspan deflection) with emphasized micro-spheres. Correctly identified micro-spheres are labelled by a blue circle, micro-spheres lost during correlation by a red circle and phantom markers by a magenta circle.

### 3.5 Inverse calculation of material properties - fitting the response curve using FE modelling

Due to the high irregularity in the specimens' shape it is not possible to use e.g. Timoshenko beam theory and calculate the stresses to plot the stress-strain curve. Instead, exact geometry of each sample must be modelled and discretized with finite elements. Boundary conditions and force must be applied with respect to the conditions in each experiment.

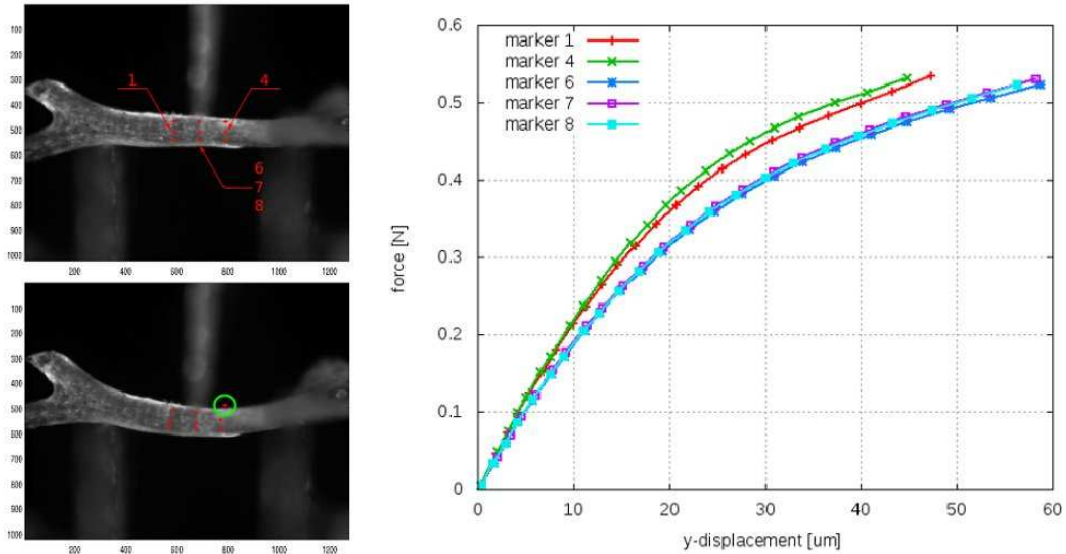


Figure 3.4: Grid of 9 points used for tracking the displacements in the three-point bending experiment and comparison of experimental force-deflection curves with those from FE simulation for the set of best-fitted material parameters (selected markers only).

To calculate the displacements at the exact positions where they were optically measured during the experiments, nodes corresponding with position of the correlation markers were selected on the surface of the model. Similarly, nodes at positions of the supports were generated in the FE models to enable application of boundary conditions at the exact locations. Similar least-squares approach of inverse calculation of material constants as described in section 2.1 is used.

Illustrative image comparing the experimental and numerical  $F - u$  curves for the best fit of material constants is given in Fig. 3.4. The results are summarized in [20, 21].

## 4 Microstructural models

### 4.1 Morphometric indices used in trabecular bone research

In the previous part of this work, methods of obtaining constitutive law for deformational description of trabecular bone at the *tissue* level have been described. It has been shown, that the overall properties of trabecular bone are influenced not only by the tissue properties, but also (and importantly) by the microstructural arrangement of the trabeculae.

In the past years, classic stereological methods were used to describe three-dimensional morphology of the bone. For this purpose, several indices has been established to characterize the microstructural arrangement of trabecular bone. Among these indices, which are used to describe the relationship between the overall bone strength and its microarchitecture, the most important are: *trabecular thickness* (**Tb.Th**), *trabecular spacing* (**Tb.Sp**). These two indices were considered to be the key indices, i.e. most influencing overall strength of trabecular bone, when measurements taken from two-dimensional images were used. In fact, histological sections were used for the purpose and with this technique, it was not possible to account fully for the three-dimensional microstructure. Moreover, it has been shown, that Tb.Th and Tb.Sp derived from anatomical locations where rod-like trabeculae prevails (vertebral bone) and from locations with dominant plate-like trabeculae (femoral head) are over- or underestimated when beam or plate models were used to estimate the average thickness and separation [22, 23]. This is the reason why 3D data must be used when fully 3D morphometric indices are to be assessed. This has been shown for the first time by Hildebrand and Rüegsegger [24] in 1997 when the authors showed, that direct 3D algorithms must be used when model-independet assessment of Tb.Th and Tb.Sp is needed. The base idea behind their approach is fitting a sphere of maximal diameter inside a space (a void in trabecular microstructure). For this purpose, they designed and implemented an efficient algorithm using distance transformation. Comparison between the results obtained from 2D histological sections and 3D measurement using micro-CT was published the same year in [25].

Using this fully 3D approach the *mean trabecular thickness* (**Tb.Th.mean**) can be reliably established. However, this is only a scalar value and can be used as a good measure for intraspecimen comparison of trabecular thickness. Tb.Th as a scalar cannot account for all structural changes that are important for e.g. monitoring structural changes over time. However, there are other structural indices, that can be measured when fully 3D image data are available. Among other indices used for morphological description of trabecular bone structure are *average trabecular number* (**Tb.N**), which is the inverse of the mean distance between the mid-axes of the microstructure. The mean distance is also used for calculation of the previously mentioned Tb.Sp



- with one change - the voxels representing non-bone parts are filled with maximal spheres.

There are other indices which can be directly determined from the 3D image data. For most of them a 3D model of the trabecular bone developed using algorithms from computer graphics must be used. First, from the thresholded images, containing only the bone a surface model is built using the Marching Cubes Algorithm [26]. Then it is easy to calculate other structural indices, such as *bone surface area* (**BS**) as the sum of all triangles used in the surface triangulation. Similarly, after the volume is filled with Delaunay tetrahedralization (see e.g. [27]), *bone volume* (**BV**) is calculated by summing the volume of all tetrahedrons inside the structure. Often, normalized indices, i.e. indices normalized to the *total volume* (**TV**) are used. These indices include bone volume to total volume (**BV/TV**), bone surface to total volume (**BS/TV**) and bone surface to volume (**BS/BV**) ratios. TV is the volume of the whole sample.

Apart from these metric indices, there exist other non-metric indices, which can be directly computed from the 3D image data. For most of these indices, *mean intercept length* (**MIL**) has been introduced. The mean intercept length is defined as the total length lines intersecting the microstructure (in one direction) divided by the number of intersections of these lines with the bone-marrow interface [28]. Using **MIL** other important geometrical parameters used to describe the anisotropy of the bone and other directional properties are defined. For instance, *degree of anisotropy* (**DA**) is geometrically defined as the ratio between the maximal and the minimal radius of the MIL ellipsoid [29]. Bone material isotropy is then defined as a situation for which DA is unity (1.0). Among other non-metric indices are *structure model index* (**SMI**) which is a good estimation of the plate-to-rod distribution characteristics, *trabecular bone pattern factor* (**TBPf**) describing the inter-trabecular connectivity and self-explanatory *connectivity density* (**Conn.D**).

In general, all of these indices can be used to describe the microstructural-mechanical relationship in trabecular bone, but none of them (nor only their combination) is comprehensive or universal. Moreover, when the post-yield deformational behaviour of trabecular bone is to be addressed, all of these indices mostly fail. Other approach to describe the quality of trabecular bone is to directly use mechanical properties, e.g. stiffness or strength. The most straightforward approach for establishing these mechanical properties is to use microstructural FE models and use inverse analysis to compute these mechanical properties for the given sample. The microFE models account with great detail for the complex microstructure and when the tissue properties are known (or expertly estimated, e.g. based on the density obtained from CT scans) the overall properties can be reliably computed. Also, nonlinear large deformation analysis can be applied [30] with nonlinear material model to simulate the post-yield behaviour.

## 4.2 Time-lapse micro-CT

Micro-CT can be used not only to reveal the microstructure of trabecular bone, but when performed in a time-lapse fashion, it can be used to provide excellent experimental data for validation

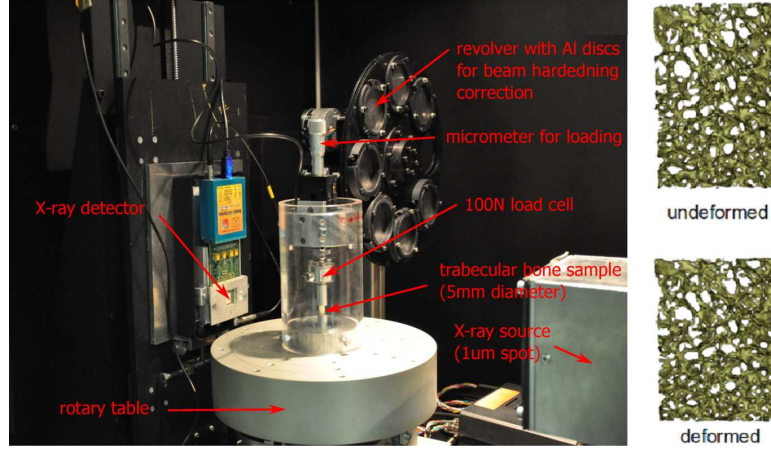


Figure 4.1: Experimental setup for the time-lapse micro-CT scanning of a loaded specimen of trabecular bone (left). Deformed microstructure in two load steps is depicted in a thin slice only (right).

of microFE models and the constitutive models used. The time-lapse micro-CT [31] is an experiment in which a specimen is repeatedly scanned in micro-CT under gradually incremented load. The result of such scanning is a sequence of three-dimensional images of the deforming microstructure. In our experiment a custom, laboratory micro-radiographic system composed of micro-focus X-ray tube and a large flat panel detector [32] was used.

To enable simultaneous loading and X-ray scanning of a specimen a custom uniaxial loading device was developed. The loading frame of the device is formed by a cylinder from material with low and homogeneous attenuation of X-rays. The loading is provided either manually by a screw or by a stepper motor. The device placed inside the X-ray shielded box is depicted in Fig. 4.1 together with resulting images of the deformed microstructure.

The specimen was gradually loaded in 6 deformation increments up to 5% overall compressive strain. The displacements were carefully controlled with high-precision linear translational stage. Time-lapse X-ray microtomography of every deformation state (including the zero deformation state) was tomographically captured a large-area flat panel with physical dimensions  $120 \times 120$  mm and pixel resolution  $2240 \times 2340$ . During the acquisition the target voltage was 70 kV and the target current was 140 mA. The initial (undeformed) state of the specimen was captured in 720 projections with angular step 0.5 and acquisition time  $40 \times 0.5$  s to get the best possible image data for development of the FE model and model used for DVC. After every loading step complete tomography using 360 projections of incrementally deforming sample was performed. Reconstruction of the internal microstructure was computed in MATLAB using a backprojection algorithm for equiangular cone-beam projection data [33] for each load increment. Both for the DVC and for the numerical modelling a FE model of the microstructure has to be developed. There are generally two options for the FE models. One can use tetrahedral elements for the discretization to obtain smooth-boundary geometrical representation or voxel elements with zigzag boundary. When tetrahedral elements are used the surface is first found using Marching Cubes Algorithm [26] which is given as a closed set of triangles describing the surface

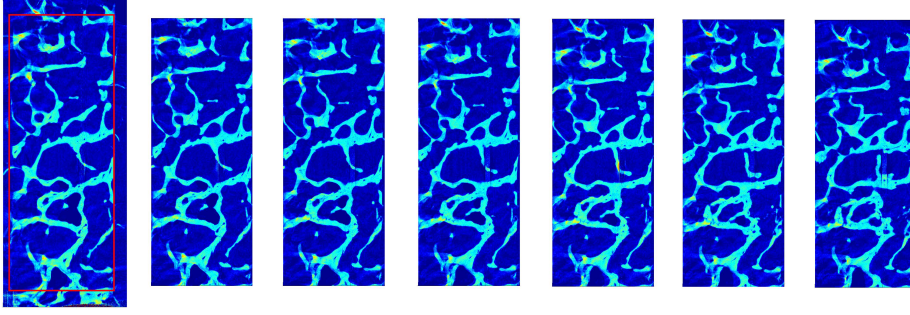


Figure 4.2: Reconstructed images of the deforming microstructure.

of the object. After some optimization and decimation (reduction of the number of triangles in the surface mesh) the volume is filled with tetrahedra using Delaunay triangulation extended to three dimensions [27]. This approach produces a large number of tetrahedra and extra requirements are needed for proper segmentation of the image data to obtain fully connected structure with non-zero volume. It is much easier to use the voxel structure (voxel is three-dimensional pixel, see Fig. 4.3) and convert directly each voxel into a linear hexahedral element. If quadratic elements are needed, the mid-side nodes are placed in the middle of the edges.

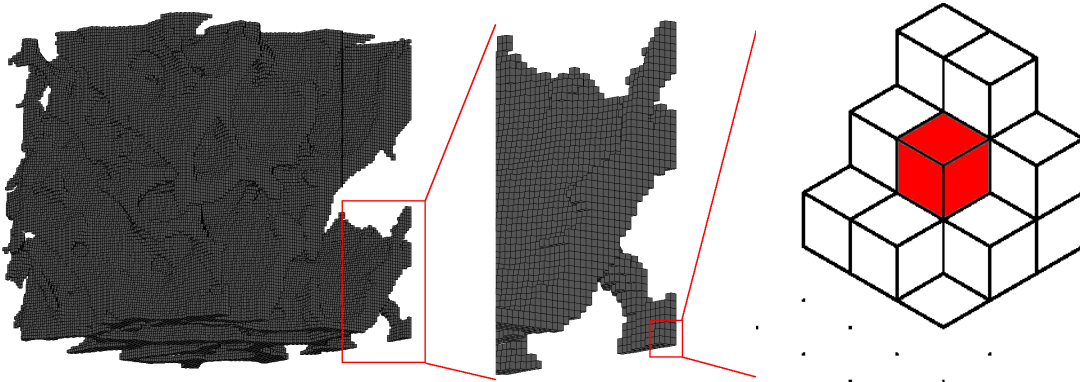


Figure 4.3: Voxel model of the trabecular bone microstructure with depicted definition of voxel as three-dimensional pixel.

## 5 Digital volume correlation

To compare the strains in the loaded sample to the values calculated by the FE analysis similar approach as the previously described image correlation can be employed. A natural extension of DIC to three dimensions can be used. This approach is sometimes called Digital Volume Correlation (DVC) [34, 35] since for the correlation subvolumes defined around the control points are used instead of subimages. Other computational principles of the method are very similar. DVC also utilizes a sequence of consecutive image data, here it is a parallelepiped volume of voxels that represents the process of the object translation and deformation. Correlation principle used to track the movement of individual subvolumes is also based on minimization of cross-correlation

coefficient. The subvolume defined around the control point must contain a distinguishable part of the object inner structure or a random pattern. This is important for tomography of an object with sparse structure. If the control point is placed in a place where no material is present, the subvolume can contain only “background” image data, i.e. air for which the X-rays attenuation is almost zero. Then the control subvolume contains only noise originating from the backprojections. Therefore, placing control points in such a place must be avoided.

This is achieved by special distribution of the control points. To force the control points to lie inside (or at the boundary) of the deforming microstructure, FE model of the microstructure is first developed and its nodes are taken as the control points. Both tetrahedral and hexahedral elements can be used.

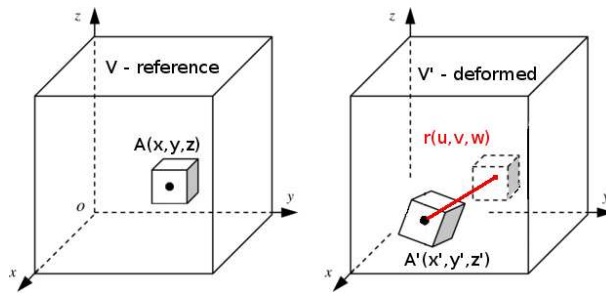


Figure 5.1: Principle of the Digital Volume Correlation. Volumetric subimage is defined in the reference volume and its transformation is sought in the deformed volume.

As the correlation algorithm normalized cross-correlation is used. The algorithm can be described in two steps: First, displacement of a voxel is evaluated using normalized cross-correlation (NCC) with result presented by an integer value. This is done using the coordinates  $(X, Y, Z)$  of the central voxel of a reference (undeformed) sub-volume data. The NCC coefficient is computed in the deformed image  $(x, y, z)$  data as a maximum defined as:

$$r = \frac{\sum_{x=1}^{x=m} \sum_{y=1}^{y=n} \sum_{z=1}^{z=o} (I_0(x, y, z) - \bar{I}_0) (I_1(x, y, z) - \bar{I}_1)}{\sqrt{\left[ \sum_{x=1}^{x=m} \sum_{y=1}^{y=n} \sum_{z=1}^{z=o} (I_0(x, y, z) - \bar{I}_0)^2 \right] \left[ \sum_{x=1}^{x=m} \sum_{y=1}^{y=n} \sum_{z=1}^{z=o} (I_1(x, y, z) - \bar{I}_1)^2 \right]}} \quad (5.1)$$

where  $I_0$  is the reference (undeformed) subvolume and  $I_1$  is the actual (deformed) subvolume, respectively. The mean values of the image intensities in the volumes are represented by the overbarred symbols  $\bar{I}_0$  and  $\bar{I}_1$ . The NCC coefficient is maximized using the steepest-gradient method. The found maximum gives the new integer coordinates  $(x, y, z)$  for which the best correlation was found. Displacement vector is at this stage calculated with pixel accuracy only:

$$u = [u, v, w]^T = [x - X, y - Y, z - Z]^T \quad (5.2)$$

The pixel accuracy is far from the requirements that one puts on the accuracy of the method. So

far, the DVC was based on the correspondence between voxels in reference and deformed volume only. There are two more changes that may occur in practical measurement data. First change is due to the nonlinear response of the X-ray detector, producing the image data. It means, the background intensity can change between the reference and deformed volume images and/or contrast may change due to the nature of the imaging device. Second, between the reference and deformed configuration, there might be not only the rigid body translation, but the subvolume may deform in shear strain, rotation, normal strain or their combinations to an irregular shape. Calculation of the subvoxel displacements must take these issues into consideration. In our algorithm, the integer values of the displacement vector are in the second step used as inputs for the further subpixel evaluation using 3D extension of Lucas-Kanade (LK) algorithm [36]. This step accounts for the deformation of the reference sub-volume (template). LK algorithm is based on the minimization of the sum of squared error between the reference and deformed sub-volumes:

$$\sum_{\vec{x}} [I_1(W(\vec{x}, \vec{p}) - I_0(\vec{x}))^2 \quad (5.3)$$

in which  $(W(\vec{x}, \vec{p}))$  describes the warp of the deformed subvolume  $I_1$  onto the reference (undeformed) subvolume  $I_0$ . Minimizing 5.3 with respect to the vector of parameters  $\vec{p}$  LK algorithm iteratively updates the position of the central voxel of the template with sub-pixel precision by employing Gauss-Newton nonlinear optimization. NCC correlation criterion offers the most robust noise-proof performance and insensitiveness to changes in illumination (in X-ray tomography this is represented by fluctuations in the X-ray source power) conditions.

The DVC method was used to calculate the displacements and strains in a loaded sample of trabecular bone. The experiment was shortly described in section 4.2. The microCT images of the undeformed sample were first used to develop a tetrahedral FE model. Nodal points of the FE model were used as the control points for DVC calculations. For each of the tetrahedral element the Green-Lagrange strain tensor was calculated using the deformation gradient tensor. The overlaid tetrahedral mesh serves not only for the calculation of the deformation tensor, but also for easy visualization of the vector and tensor fields and for fast and direct comparison with results of numerical simulations. The numerical simulations can use the existing tetrahedral mesh or the mesh can be easily refined/coarsened if needed.

Example of a comparison between the experimentally measured strain distribution in a loaded sample and numerical simulation can be seen in Fig. 5.2. For the DVC only a thin slice ( $700 \times 40 \times 1575$  pixels) defined in the central part of the volumetric data was selected (depicted with a red rectangle). Displacement and strain fields were calculated for each deformation state. Evolution of the displacements during the experiment can be easily compared to values from numerical simulation. Detailed information about the experimental results can be found in [37].

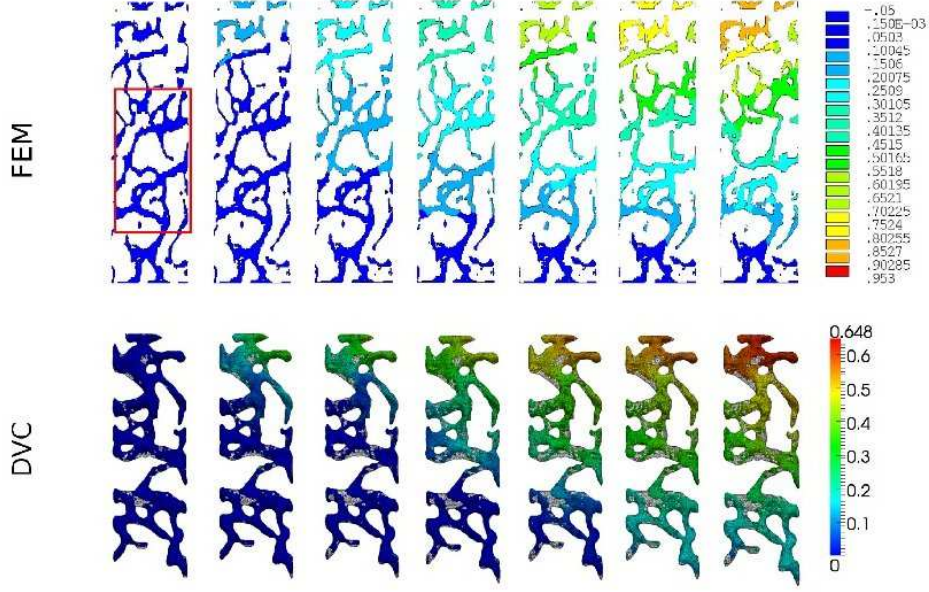


Figure 5.2: Comparison between the experimental and numerical results – displacement fields for all the considered deformational states. From top to bottom: a) FE results, b) displacements calculated with DVC from the image data.

## 6 Inverse estimation of whole bone stiffness

### 6.1 Voxel and tetrahedral micro-FE models

Inverse estimation of material properties (namely stiffness and strength) of trabecular bone using FE models of its microstructure is important not only as a nondestructive tool for early prediction of osteoporotic fracture, but can be successfully applied in other research areas, e.g. in animal models to study effect of various factors on bone formation. These microstructural FE models are used to perform a numerical simulation of mechanical experiment. Usually, the micro-FE model is subjected to unit load in three mutually perpendicular directions and elastic constants are determined from the 'virtual experiment'. The material properties at the tissue level are considered homogeneous and usually determined from nanoindentation [38, 39] or if nanoindentation is not possible, expertly estimated.

The micro-FE models assume that orthotropic behaviour of trabecular bone is given only by the microstructural arrangement of the trabecular network and at the level of single trabecula the properties can be considered isotropic. Recent studies showed slight anisotropy in elastic properties of trabecular bone [40]. In their work, microindentation with depth equal to  $2.5 \mu\text{m}$  was used in six regions of interest – axial and transverse sections in the same trabeculae. In axial direction indentation modulus significantly higher than in transverse direction. It was concluded by the authors, that trabeculae can be considered (generally) transversely anisotropic, at least in the structure of vertebral bodies. However, no other study has been published so far proving the

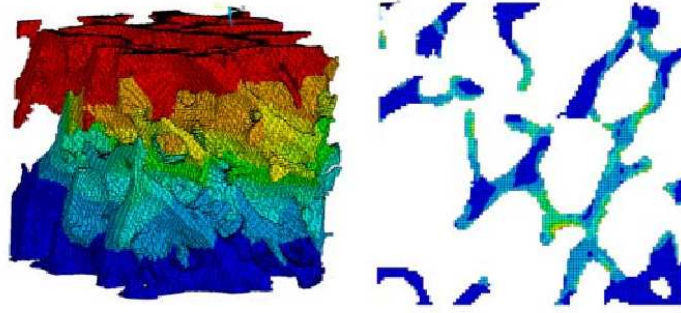


Figure 6.1: Voxel model of a cubic sample of trabecular bone in a virtual compression test. Field of vertical displacements is rendered.

general anisotropy in the indentation modulus (this is in contrary to the compact bone. Here the anisotropy is present originating from the anisotropy of single osteon [3]).

Nowadays, the micromechanical FE models of trabecular bone microstructure, either voxel-based or tetrahedral are almost considered as de-facto standard tool for estimation of overall stiffness of trabecular bone. It has been shown, that if requirements for the resolution of the images are met and when the tissue material properties are evaluated using nanoindentation (both dry and wet samples have been used and successfully tested) the micro-FE models are able to predict the bone (orthotropic) elastic properties with great success [16].

## 6.2 Micro-FE models of whole bones

With the growth of computer power it is nowadays possible to solve large systems of algebraic equations. This enables to develop very large (and/or very detailed) FE models. In early 2000s detailed FE models of trabecular bone microstructure were used for inverse determination of their overall mechanical properties [41, 42]. In these microstructural models, tissue material properties are usually assumed to be isotropic and homogeneous and are determined using either nanoindentation [18, 19, 13] or from micromechanical tests performed on individual trabeculae [43, 44, 26]. Until the use of parallel computers the micro-FE models involved only small volume of trabecular bone (usually cylindrical core samples) [45], and inverse estimation of the overall stiffness and strength of whole bones was not possible until the late 2000s [46, 47].

With growing availability of parallel computers and parallel solvers (both iterative and direct) together with advancement in X-ray imaging systems, particularly with growing resolution of X-ray flat panel detectors it has become possible to develop and solve high-resolution micro-FE models of whole bones which take into account the real microstructure of the trabecular bone. The microstructure must be captured by these models with great precision which leads to FE models with very large number of elements (about 1 million elements per cubic cm at  $50\text{ }\mu\text{m}^3$  resolution). This requires to solve approximately  $10^7 - 10^8$  equations to perform FE analysis of whole bone samples (e.g. vertebral bodies). It is virtually impossible to model the whole bone using tetrahedral elements (a closed surface is needed) and therefore voxel-based microstructural



FE models are used exclusively to calculate inversely the overall mechanical properties of whole bones.

### 6.3 Development of the micro-FE voxel model of rat vertebra

To demonstrate the possibility to use micro-FE models of whole bones for estimation of their overall stiffness and strength a rat vertebra has been microtomographically scanned. The FE model capturing its microstructure in great detail has been developed using voxel elements. For the scanning a microfocus X-ray source together with large-area flat panel X-ray detector with resolution  $2368 \times 2240$  pixels and physical dimensions  $120 \times 120$  mm was used. Scanning sequence consisted of 360 scans with  $0.5^\circ$  step.

The cross-sectional image data were reconstructed from the sinograms using FBP (filtered back-projection) algorithm taking the cone-beam geometry of the scanning setup into account. Only the vertebral body was considered in the micro-FE model. Both the cortical shell and internal trabecular structure was modelled using voxel-based approach. In the stiffness calculation, both endplates and the posterior processes were also modelled using voxel elements. This simplifies the load application and application of boundary conditions. These simplifications enabled direct conversion from the micro-CT image data to the micro-FE model. Final micro-FE model of the rat vertebra, consisting of more than 4 million hexahedral elements is shown in Fig. 6.2.

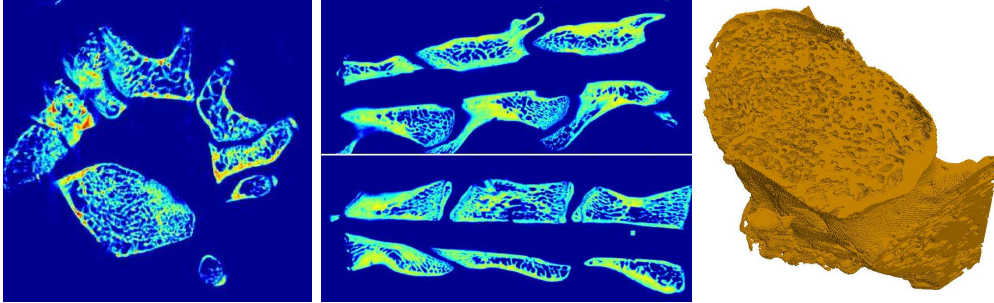


Figure 6.2: Cross-sectional images (left) of the micro-CT data from which the voxel FE model of the rat vertebral body was developed (right).

### 6.4 Inverse calculation of the vertebral body stiffness

To compute the overall stiffness of the vertebral body in the infero-superior direction a unit displacement has been prescribed on the top surface of the vertebral body. The lower surface of the body was fixed (all nodes with minimal z-coordinate were prescribed zero displacements in three directions). Based on our previous nanoindentation results [13] following (tissue-level) material properties were prescribed: Young's modulus of elasticity  $E_{\text{tiss}}=15$  GPa, Poisson's ratio:  $\mu_{\text{tiss}}=0.2$ . Aside the model of the vertebral body,  $100 \times 100 \times 100$  voxels were selected in the middle part for easy comparison of orthotropic elastic properties. Total number of nodes was 4,791,142



with total number of unknowns larger than  $14 \cdot 10^6$ . Prior the computations, the FE model was verified for mesh connectivity.

## 6.5 Parallel PCG solver

The critical part of the FE computation of such a large model is the solver. For the current micro-FE analyses of voxel models of trabecular bone is one level element-by-element preconditioned conjugate gradient (EBE-PCG) [48] considered as the most frequently used solver. The solver takes advantage of the identical size of every element in the voxel model (every element has exactly the same stiffness matrix) and it is very memory efficient (it does not assemble the global stiffness matrix) since it requires only a matrix-vector product. However, due to its slow convergence and poor scalability, this solver is efficient only for moderate-sized problems (under 1 million elements) and can be successfully used for the solution of small-volume samples of trabecular bone. For large models of whole bones or for nonlinear material models (plasticity) this solver is inefficient [49]. For our computations, parallel PCG solver with  $1 \cdot 10^{-8}$  tolerance without the EBE preconditioning was used. More on solution and scalability of the parallel solver can be found in [50].

## 6.6 Experimental evaluation of the vertebral stiffness

The endplates of the vertebra were fixed in a low-shrinkage epoxy resin. The vertebra was kept frozen and prior the experiment thawed to room temperature. The specimen was placed in our loading device. The overall strain was measured optically as to exclude the deformation of the epoxy resin. The experimental setup is depicted in Fig. 6.3.



Figure 6.3: Compression test of the L<sub>2</sub> rat vertebra. Experimental setup (left). The specimen observed with 5 MPix CCD camera is shown for two loading states (right). The upper and lower endplates are fixed in low-shrinkage epoxy resin.

From the recorded images, deformation in vertical direction was computed using DIC. Two rows of correlation markers were selected in the undeformed image as to exclude the portion of the vertebra fixed in the epoxy resin. Deformation was also measured from the displacement of the

loading platten and the influence of the epoxy resin was found approximately 10%. The overall stress was computed as the applied force divided by the cross-sectional area. The area was computed using image analysis of the mid-height cross-section. Microtomographic image was used for the evaluation.

Numerically assessed overall stiffness of the rat's vertebra was compared to the value measured experimentally. The results were in good agreement, however, the details exceed limited length of this text, the reader is kindly asked to see [51].

## 7 Conclusions

Presented experimental and numerical methods help to understand not only the relationship between the microstructural and macrostructural properties of trabecular bone, but also enable to rigorously evaluate properties of bone substitutes and artificially prepared bone. One of the research areas in which presented results are already finding their place is tissue engineering. Here it is essential to compare the material properties of trabecular bone before and after an orthopaedic therapy. This might include research in stem cell therapy, pre-clinical evaluation of primary fixation of implants and other. Using the laboratory models it would be possible to evaluate the outcome *nondestructively* using the micro-CT. With the help of the inverse micro-FE modelling it is possible to get important information not only qualitatively about the microstructure (stereological indices), but also quantitative information about the material (stiffness, strength).

Micro-CT can be helpful for evaluation of the safety and efficacy of bioartificial graft materials. An attempt to utilize micro-CT to evaluate the performance of a scaffold material based on a hydroxyapatite combined with human mesenchymal stem cells (MSCs) in a rat model of vertebral body defects was performed [52]. A defect in the body of the L2 vertebra was prepared and either left to spontaneous healing, implanted with augmentation material alone, or with augmentation material with different number of MSCs. Apart from routine histological measurement histomorphometry and microCT measurements were performed to assess the performance of the different healing conditions. The ability of micro-CT to visualize the newly formed bone in 3D (for which spatial measurements and characterization of the microstructure is easy) is demonstrated in Fig. 7.1. In the study it was concluded, that MSCs combined with a hydroxyapatite scaffold improved the repair of the vertebral bone defect.

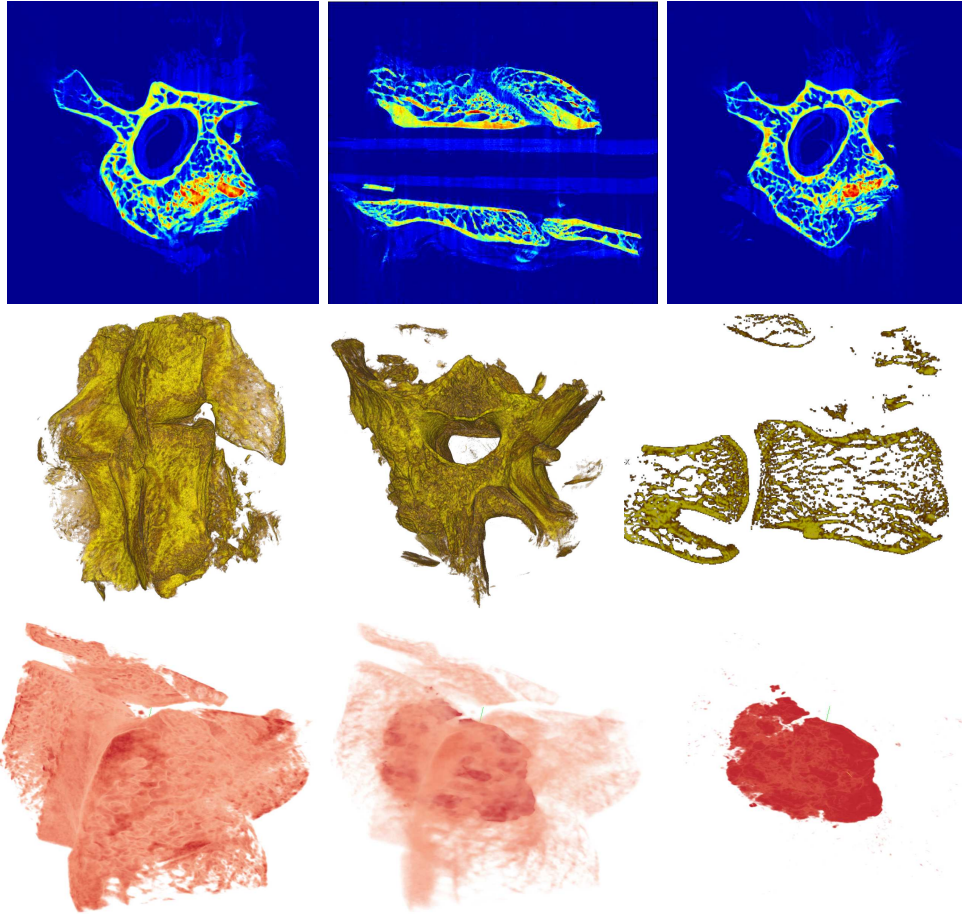


Figure 7.1: Visualization of the newly formed bone in rat model of vertebral body defect. First row: cross-sectional slices can be computed at any location and the newly-formed bone easily distinguished from the old one. Second row: the same can be done in 3D using various rendering techniques. Third row: the new bone can be properly segmented and its volume can be directly calculated.

There are also other areas where the described methods are fully applicable. One good example is evaluation of primary stability of orthopaedic or dental implants. In this research, combination of time-lapse micro-CT and numerical modelling (voxel-based microFE models) would provide deep insight into the problematic of implant loosening. One rapidly growing area of research is focused on dental implant surface technology, e.g. endosseous dental implant surfaces embellished with nanoscale to microscale modifications to the implant's surface. With micro-CT measurements performed in timeline the implant can be observed and its performance under various scenarios can be properly evaluated.

**ACKNOWLEDGEMENTS** Support of the Grant Agency of the Czech Republic (Research Project 105/10/2305) and Grant Agency of the Academy of Sciences of the Czech Republic (AV0Z20710524) is gratefully acknowledged.

# Bibliography

- [1] J. Y. Rho, P. Zioupos, J. D. Currey, and G. M. Pharr, “Variations in the individual thick lamellar properties within osteons by nanoindentation,” *Bone*, vol. 25, no. 3, pp. 295 – 300, 1999.
- [2] C. E. Hoffer, X. E. Guo, P. K. Zysset, and S. A. Goldstein, “An application of nanoindentation technique to measure bone tissue Lamellae properties,” *Journal of Biomechanical Engineering*, vol. 127, no. 7, pp. 1046 – 1053, 2005.
- [3] A. G. Reisinger, D. H. Pahr, and P. K. Zysset, “Principal stiffness orientation and degree of anisotropy of human osteons based on nanoindentation in three distinct planes,” *Journal of Mechanical Behaviour of Biomedical Materials*, vol. 4, no. 8, pp. 2113 – 2127, 2011.
- [4] S. A. Goldstein, “The mechanical properties of trabecular bone: Dependence on anatomic location and function,” *Journal of Biomechanics*, vol. 20, no. 11 - 12, pp. 1055 – 1061, 1987.
- [5] T. M. Keaveny and W. C. Hayes, “A 20-year perspective on the mechanical properties of trabecular bone,” *Journal of Biomechanical Engineering*, vol. 115, no. 4B, pp. 534 – 542, 1993.
- [6] C. D. Wright, E. O. Crawley, W. D. Evans, N. J. Garrahan, R. W. Mellish, P. I. Croucher, and J. E. Compston, “The relationship between spinal trabecular bone mineral content and iliac crest trabecular bone volume,” *Calcified Tissue International*, vol. 46, no. 3, pp. 162 – 165, 1990.
- [7] P. K. Zysset, X. E. Guo, C. E. Hoffer, K. E. Moore, and S. A. Goldstein, “Mechanical properties of human trabecular bone lamellae quantified by nanoindentation,” *Technology and Health Care*, vol. 6, no. 5 - 6, pp. 429 – 432, 1998.
- [8] J. S. Nyman, A. Roy, X. Shen, R. L. Acuna, J. H. Tyler, and X. Wang, “The influence of water removal on the strength and toughness of cortical bone,” *J Biomech*, vol. 39, no. 5, pp. 931–938, 2007.
- [9] W. C. Oliver and G. M. Pharr *Journal of Materials Research*, vol. 7, no. 6, pp. 1564 – 1583, 1992.
- [10] G. M. Pharr, W. C. Oliver, and F. R. Brotzen, “On the generality of the relationship among contact stiffness, contact area, and the elastic modulus during indentation,” *Journal of Materials Research*, vol. 7, no. 3, pp. 613 – 617, 1992.
- [11] E. J. Pavlina and C. J. V. Tyne, “Correlation of Yield Strength and Tensile Strength with Hardness for Steels,” *Journal of Materials Engineering and Performance*, vol. 17, no. 6, pp. 888 – 893, 2008.
- [12] C. Chen, *2-D Finite element modeling for nanoindentation and fracture stress analysis*. PhD thesis, University of South Florida, 2009. PhD Thesis.
- [13] O. Jiroušek, J. Němeček, D. Kytýř, J. Kunecký, P. Zlámal, and T. Doktor, “Nanoindentation of Trabecular Bone – Comparison with Uniaxial Testing of Single Trabecula,” *Chemické Listy*, vol. 105, no. s5, pp. 668 – 671, 2011.

- [14] O. Jiroušek, D. Kytýř, P. Zlámal, T. Doktor, J. Šepitka, and J. Lukeš, “Use of Modulus Mapping Technique to Investigate Cross-sectional Material Properties of Extracted Single Human Trabeculae,” *Chemické listy*, vol. 106, no. S3, pp. 442 – 445, 2012.
- [15] E. Verhulp, B. van Rietbergen, and R. Muller, “Indirect determination of trabecular bone effective tissue failure properties using micro-finite element simulations,” *Journal of Biomechanics*, vol. 41, no. 7, pp. 1479 – 1485, 2008.
- [16] U. Wolfram, H.-J. Wilke, and P. K. Zysset, “Valid micro finite element models of vertebral trabecular bone can be obtained using tissue properties measured with nanoindentation under wet conditions,” *J Biomech*, vol. 43, no. 9, pp. 1731 – 1737, 2010.
- [17] J. Norman, J. G. Shapter, K. Short, L. J. Smith, and N. L. Fazzalari, “Micromechanical properties of human trabecular bone: A hierarchical investigation using nanoindentation,” *Journal of Biomedical Materials Research Part A*, vol. 87, no. 1, pp. 196 – 202, 2008.
- [18] J.-Y. Rho, T. Y. Tsui, and G. M. Pharr, “Elastic properties of human cortical and trabecular lamellar bone measured by nanoindentation,” *Biomaterials*, vol. 18, no. 20, pp. 1325 – 1330, 1997.
- [19] P. K. Zysset, X. E. Guo, C. E. Hoffler, K. E. Moore, and S. A. Goldstein, “Elastic modulus and hardness of cortical and trabecular bone lamellae measured by nanoindentation in the human femur,” *Journal of Biomechanics*, vol. 32, no. 10, pp. 1005 – 1012, 1999.
- [20] O. Jiroušek, D. Kytýř, T. Doktor, J. Dammer, and F. Krejčí, “Displacement tracking in single human trabecula with metal-plated micro-spheres using X-ray radiography imaging,” *Journal of Instrumentation*, vol. 8, no. 02, p. C02041, 2013.
- [21] P. Zlámal, O. Jiroušek, T. Doktor, and D. Kytýř, “Modelling Elasto-plastic Behaviour of Human Single Trabecula - Comparison with Bending Test,” *Journal of Biomechanics*, vol. S1, no. 12, p. S479, 2012.
- [22] A. Odgaard, “Three-dimensional methods for quantification of cancellous bone architecture,” *Bone*, vol. 20, pp. 315 – 328, 1997.
- [23] J. Day and et al., “Parallel Plate Model for Trabecular Bone Exhibits Volume Fraction-Dependent Bias,” *Bone*, vol. 27, no. 5, pp. 715 – 720, 2000.
- [24] T. Hildebrand and P. Rüegsegger, “A new method for the model-independent assessment of thickness in three-dimensional images,” *Journal of Microscopy*, vol. 185, no. 1, pp. 67 – 75, 1997.
- [25] D. Chappard, E. Legrand, and et al., “Measuring trabecular bone architecture by image analysis of histological sections,” *Microscopy and Analysis*, vol. 13, pp. 23 – 25, 1997.
- [26] W. E. Lorensen and H. E. Cline, “Marching cubes: A high resolution 3d surface construction algorithm,” *Computer Graphics*, vol. 21, no. 4, pp. 163 – 169, 1987.
- [27] S. Gosselin and C. Ollivier-Gooch, “Constructing constrained delaunay tetrahedralizations of volumes bounded by piecewise smooth surfaces,” *International Journal of Computational Geometry & Applications*, vol. 21, no. 05, pp. 571 – 594, 2011.
- [28] A. Odgaard, E. B. Jensen, and H. J. Gundersen, “Estimation of structural anisotropy based on volume orientation. A new concept,” *Journal of Microscopy*, vol. 162, pp. 149 – 162, 1990.
- [29] T. P. Harrigan and R. W. Mann, “Characterization of microstructural anisotropy in orthotropic materials using a second rank tensor,” *Journal of Materials Science*, vol. 19, pp. 761 – 767, 1984.

- [30] G. Bevill, S. K. Eswaran, and et al., “Influence of bone volume fraction and architecture on computed large-deformation failure mechanisms in human trabecular bone,” *Bone*, no. 39, pp. 1218 – 1225, 2006.
- [31] A. Nazarian and R. Müller, “Time-lapsed microstructural imaging of bone failure behavior,” *Journal of Biomechanics*, vol. 37, no. 1, pp. 55 – 65, 2004.
- [32] J. Jakubek, T. Holy, M. Jakubek, D. Vavrik, and Z. Vykydal, “Experimental system for high resolution x-ray transmission radiography,” *Nuclear Instruments and Methods in Physics Research Section A: Accelerators, Spectrometers, Detectors and Associated Equipment*, vol. 563, no. 1, pp. 278 – 281, 2006.
- [33] D. Vavřík and P. Soukup, “Metal grain structure resolved with table-top micro-tomographic system,” *Journal of Instrumentation*, vol. 6, no. 11, p. C11034, 2011.
- [34] T. C. Chu, W. F. Ranson, M. A. Sutton, and W. H. Peters, “Applications of digital-image-correlation techniques to experimental mechanics,” *Experimental Mechanics*, vol. 25, p. 232, 1985.
- [35] B. K. Bay, T. S. S. D. P. Fyhrie, and M. Saad, “Digital volume correlation: Three-dimensional strain mapping using X-ray tomography,” *Experimental Mechanics*, vol. 39, no. 3, pp. 217 – 226, 1999.
- [36] B. D. Lucas and T. Kanade, “An iterative image registration technique with an application to stereo vision,” *Proceedings of the Image Understanding Workshop*, vol. 40, pp. 121–130, 1981.
- [37] P. Zlamal, O. Jirousek, T. Doktor, T. Fila, and D. Kytýr, “Compressive behaviour of trabecular tissue - finite element modelling and comparison using digital volume correlation,” (Cagliari, Sardinia, Italy), 2013. to appear.
- [38] B. van Rietbergen, A. Odgaard, J. Kabel, and R. Huiskes, “Direct mechanics assessment of elastic symmetries and properties of trabecular bone architecture,” *Journal of Biomechanics*, vol. 29, no. 12, pp. 1653 – 1657, 1996.
- [39] Y. Chevalier, D. Pahr, H. Allmer, M. Charlebois, and P. Zysset, “Validation of a voxel-based FE method for prediction of the uniaxial apparent modulus of human trabecular bone using macroscopic mechanical tests and nanoindentation,” *Journal of Biomechanics*, vol. 40, no. 15, pp. 3333 – 3340, 2007.
- [40] U. Wolfram, H. Wilkea, and P. K. Zysset, “Transverse isotropic elastic properties of vertebral trabecular bone matrix measured using microindentation (effects of age, gender and vertebral level),” *Bone*, vol. 44, no. 12, pp. S392 – S393, 2009.
- [41] B. V. Rietbergen, R. Muller, D. Ulrich, P. Rueggsegger, and R. Huiskes, “Tissue stresses and strain in trabeculae of a canine proximal femur can be quantified from computer reconstructions,” *Journal of Biomechanics*, vol. 32, no. 2, pp. 165 – 173, 1999.
- [42] Glen L. Niebur, Michael J. Feldstein, Jonathan C. Yuen, Tony J. Chen, and Tony M. Keaveny, “High-resolution finite element models with tissue strength asymmetry accurately predict failure of trabecular bone,” *Journal of Biomechanics*, vol. 33, pp. 1575–1583, Dec. 2000.
- [43] R. Jungmann, M. E. Szabo, G. Schitter, R. Y.-S. Tang, D. Vashishth, P. K. Hansma, and P. J. Thurner, “Local strain and damage mapping in single trabeculae during three-point bending tests,” *Journal of the Mechanical Behavior of Biomedical Materials*, vol. 4, no. 4, pp. 523 – 534, 2011.

- [44] T. Doktor, O. Jirousek, D. Kytyr, P. Zlamal, and I. Jandejsek, “Real-time X-ray microradiographic imaging and image correlation for local strain mapping in single trabecula under mechanical load,” *Journal of Instrumentation*, vol. 6, no. 11, 2011. Art.No. C11007.
- [45] R. Muller and P. Rueggsegger, “Three-dimensional finite element modelling of non-invasively assessed trabecular bone structures,” *Medical Engineering and Physics*, vol. 17, no. 2, pp. 126 – 133, 1995.
- [46] J. A. MacNeil and S. K. Boyd, “Bone strength at the distal radius can be estimated from high-resolution peripheral quantitative computed tomography and the finite element method,” *Bone*, vol. 42, no. 6, pp. 1203 – 1213, 2008.
- [47] S. K. Eswaran, H. H. Bayraktar, M. F. Adams, A. Gupta, P. F. Hoffmann, D. C. Lee, P. Papadopoulos, and T. M. K.-. eny, “The micro-mechanics of cortical shell removal in the human vertebral body,” *Computer Methods in Applied Mechanics and Engineering*, vol. 196, no. 3132, pp. 3025 – 3032, 2007.
- [48] T. J. R. Hughes, R. M. Ferencz, and J. O. Hallquist, “Large-scale vectorized implicit calculation in solid mechanics on a Cray X-MP/48 utilizing EBE preconditioned conjugate gradients,” *Computer Methods in Applied Mechanics and Engineering*, vol. 61, pp. 215 – 248, 1987.
- [49] B. van Rietbergen, R. Huiskes, F. Eckstein, and P. Rueggsegger, “Trabecular bone tissue strains in the healthy and osteoporotic human femur,” *Journal of Bone and Mineral Research*, vol. 18, no. 10, pp. 1781 – 1788, 2003.
- [50] O. Jiroušek, Zlámál, and P, “Large-scale micro-finite element simulation of compressive behavior of trabecular bone microstructure,” *Engineering Mechanics 2012*, pp. 543 – 549, 2012.
- [51] O. Jirousek, P. Zlamal, I. Jandejsek, and D. Kytyr, “Inverse estimation of rat vertebrae stiffness using large-scale micro-structural FE models,” (Cagliari, Sardinia, Italy), 2013. to appear.
- [52] V. Vaněček, K. Klíma, A. Kohout, O. Jiroušek, J. Štulík, and E. Syková, “Mesenchymal stem cells promote bone tissue regeneration in a preclinical rat model of vertebral body defect,” *Journal of Tissue Engineering and Regenerative Medicine*, vol. 6 - SI, no. Supplement - 1, 2012.

**Doc. Ing. Ondřej Jiroušek, Ph.D.**

**Datum narození:** 6.6.1974

#### **Dosažené vzdělání**

- 2007 Doc., Fakulta dopravní ČVUT v Praze, název habilitační práce: “Application of the Finite Element Method for Head Injury Assessment in Traffic Accidents.”
- 2004 Ph.D., Fakulta stavební, ČVUT v Praze, název disertační práce: “Mathematical Models in Biomechanics Constructed on Basis of Data Obtained from Computer Tomography.”
- 1999 Ing., Fakulta stavební, ČVUT v Praze, název diplomové práce: “Napěťová analýza dlahy pro artrodézu zápěstí.”

#### **Pozice**

- 2008– vedoucí Oddělení biomechaniky, Ústav teoretické a aplikované mechaniky, Akademie věd České republiky, v.v.i.
- 2007– docent, Ústav mechaniky a materiálu, Fakulta dopravní, ČVUT v Praze
- 1999– Laboratoř biomechaniky, Ústav teoretické a aplikované mechaniky, Akademie věd České republiky, v.v.i. (od 2002 vedoucí Laboratoře biomechaniky)

#### **Hlavní vědecké aktivity**

Mechanika trabekulární kosti, zkoušení biologických struktur a materiálů (mikrotomografie vzorku pod zatížením v reálném čase), optické metody pro měření deformace, numerické metody mechaniky aplikované na biomechanické problémy (metoda konečných prvků), biomechanika částí lidského skeletu a jeho umělých náhrad.

#### **Ocenění**

- 2005 cena profesora Valenty a profesora Čiháka, udělená Českou společností pro biomechaniku za nejlepší PhD práci

#### **Udělené granty**

- P105/12/0824 – Němeček, J., Jiroušek, O.: Determination of Structural and Mechanical Properties of Metal Foams Using Nanoindentation, Computer tomography and Microstructural FEM models (spoluřešitel, 2012-2014, celkový rozpočet 8.7M CZK)
- P105/10/2305 -Jiroušek, O.: Morphometry and mechanical properties of trabecular bone assessed by methods of micromechanics and numerical modelling (hlavní řešitel, 2010-2013, budget 2.4M CZK)
- GP103/07/P483 -Jiroušek, O.: High-resolution microCT FE-models of cancellous bone structure and their application to selected problems in biomechanics (hlavní řešitel, 2007-2009, budget 0.7M CZK)



- FP6 program INNOTRACK (Development of cost-effective high performance track infrastructure for heavy rail systems)(člen týmu spoluřešitele za ČVUT zodpovědný za část numerického modelování, 2007-2009, celkový rozpočet 18.6M EUR, z toho rozpočet pro ČVUT 0.5M EUR)

### **Publikační činnost, členství v edičních radách, organizačních výborech**

- autor 18 impaktovaných článků v mezinárodních vědeckých časopisech, 7 článků v recenzovaných časopisech, 3 kapitol v zahraničních knihách, více než 60 vědeckých článků prezentovaných na mezinárodních konferencích a více než 40 vědeckých článků prezentovaných na národních konferencích, 2 software a 3 funkčních vzorků.
- předseda organizačního výboru mezinárodní konference s názvem “XIIIth Bilateral Czech/German Bilateral Symposium”, Telč, ČR, 2012
- předseda organizačního výboru mezinárodní konference s názvem “XIIth Bilateral Czech/German Bilateral Symposium”, Bremen, Německo, 2010
- člen Ediční rady mezinárodní konference The Eight International Conference on Engineering Computational Technology, Dubrovnik, Croatia, 2012
- člen Ediční rady mezinárodní konference ECT2010: The Seventh International Conference on Engineering Computational Technology, Valencia, Spain, 2010
- člen organizačního výboru mezinárodní konference “XIth Bilateral Czech/German Bilateral Symposium”, Liblice, ČR, 2008
- člen organizačního výboru mezinárodní konference “IXth Bilateral Czech/German Bilateral Symposium”, Tábor, ČR, 2004
- editor “Experimental Stress Analysis Conference Proceedings”, Tábor, Czech Republic, 2001
- člen České společnosti pro mechaniku
- člen Mezinárodní společnosti pro biomechaniku (International Society for Biomechanics)
- člen Evropské společnosti pro biomechaniku (European Society for Biomechanics)

### **Deset vybraných nejvýznamnějších publikací:**

1. Jiroušek, O. (2012). Nanoindentation of Human Trabecular Bone – Tissue Mechanical Properties Compared to Standard Engineering Test Methods. In: Nanoindentation in Materials Science (pp. 259–284). InTech Publishing. (kapitola v knize)

2. Vaněček, V., Klíma, K., Kohout, A., Jiroušek, O., Štulík, J., Syková, E. Mesenchymal stem cells promote bone tissue regeneration in a preclinical rat model of vertebral body defect, *Journal of Tissue Engineering and Regenerative Medicine*, 6(SI) Supplement: 1, 2012. IF 3.278
3. Doktor, T., Jiroušek, O., Kytýř, D., Zlámál, P., Janděšek, I. Real-time X-ray microradiographic imaging and image correlation for local strain mapping in single trabecula under mechanical load (2011) *Journal of Instrumentation*, 6 (11), art. no. C11007. IF 1.869
4. Jiroušek, O., Zlámál, P., Kytýř, D., Kroupa, M. Strain analysis of trabecular bone using time-resolved X-ray microtomography (2011) *Nuclear Instruments and Methods in Physics Research, Section A: Accelerators, Spectrometers, Detectors and Associated Equipment*, 633 (SUPPL. 1), pp. S148-S151. IF 1.207
5. Jiroušek, O., Janděšek, I., Vavřík, D. Evaluation of strain field in microstructures using micro-CT and digital volume correlation (2011) *Journal of Instrumentation*, 6 (1), art. no. C01039. IF 1.869
6. Kytýř, D., Jiroušek, O., Dammer, J. High resolution X-ray imaging of bone-implant interface by large area flat-panel detector (2011) *Journal of Instrumentation*, 6 (1), art. no. C01038. IF 1.869
7. Jiroušek, O., Doktor, T., Kytýř, D., & Zlámál, P. (2012). X-ray Radiography of Three-Point Bending of Single Human Trabecula. *Journal of Biomechanics*, 45(S1), S261. IF 2.434
8. Zlámál, P., Jiroušek, O., Doktor, T., & Kytýř, D. (2012). Modelling Elasto-plastic Behaviour of Human Single Trabecula – Comparison with Bending Test. *Journal of Biomechanics*, 45(S1), S479. IF 2.434
9. Vavřík, D., Dammer, J., Jakůbek, J., Jeon, I., Jiroušek, O., Kroupa, M., & Zlámál, P. (2011). Advanced X-ray radiography and tomography in several engineering applications. *Nuclear Instruments and Methods in Physics Research Section A: Accelerators, Spectrometers, Detectors and Associated Equipment*, 633, S152–S155. IF 1.207
10. Jiroušek, O., Zlámál, P., Kytýř, D., & Kroupa, M. (2010). Strain analysis of trabecular bone using time-resolved X-ray microtomography. *Nuclear Instruments and Methods in Physics Research Section A: Accelerators, Spectrometers, Detectors and Associated Equipment* IF 1.207